

Rippled area formed by surface plasmon polaritons upon femtosecond laser double-pulse irradiation of silicon: the role of carrier generation and relaxation processes

Thibault J.-Y. Derrien · Jörg Krüger · Tatiana E. Itina ·
Sandra Höhm · Arkadi Rosenfeld · Jörn Bonse

Received: date / Accepted: date

Abstract The formation of laser-induced periodic surface structures (LIPSS, ripples) upon irradiation of silicon with multiple irradiation sequences consisting of femtosecond laser pulse pairs (pulse duration 150 fs, central wavelength 800 nm) is studied numerically using a rate equation system along with a two-temperature model accounting for one- and two-photon absorption and subsequent carrier diffusion and Auger recombination processes. The temporal delay between the individual equal-energy fs-laser pulses was varied between 0 and ~ 4 ps for quantification of the transient carrier densities in the conduction band of the laser-excited silicon. The results of the numerical analysis reveal the importance of carrier generation and relaxation processes in fs-LIPSS formation on silicon and quantitatively explain the two time constants of the delay dependent decrease of the Low-Spatial-Frequency LIPSS (LSFL) area observed experimentally. The role of carrier generation, diffusion and recombination are quantified individually.

DOI: 10.1007/s00339-013-8205-2. The final publication is available at <http://link.springer.com>.

Keywords Laser-induced periodic surface structure (LIPSS) · Femtosecond laser · Silicon · Surface-Plasmon-Polariton · Double-pulse

Thibault J.-Y. Derrien, Jörg Krüger, Jörn Bonse
BAM Bundesanstalt für Materialforschung und -prüfung, Unter den Eichen 87, D-12205 Berlin, Germany
Tel.: +49-(0)30-8104-3562
Fax: +49-(0)30-8104-1827
E-mail: thibault.derrien@gmail.com

Tatiana E. Itina
Laboratoire Hubert Curien (LabHC), UMR CNRS 5516 - Université Jean Monnet Bat. F, 18 rue du Professeur Benoit Lauras, 42000 Saint-Etienne, France

Sandra Höhm, Arkadi Rosenfeld
Max-Born-Institut für Nichtlineare Optik und Kurzzeitspektroskopie (MBI), Max-Born-Straße 2A, D-12489 Berlin, Germany

PACS 79.20.Ds · 73.20.Mf · 06.60.Jn · 68.35.Bg

1 Introduction

The irradiation of solids with multiple linear polarized femtosecond laser pulses at fluences close to the damage threshold leads to the formation of laser-induced periodic surface structures (LIPSS) on the surface of almost all materials [1–4]. For strong absorbing materials such as metals or semiconductors, in most cases low-spatial-frequency LIPSS (LSFL) are observed with a period Λ_{LSFL} close to the irradiation wavelength λ [1,2,4]. These LSFL are generated by interference of the incident laser beam with a surface electromagnetic wave (SEW) generated at a rough surface [5,6].

On silicon, predominantly LSFL were observed after low repetition rate (≤ 1 kHz) Ti:Sapphire femtosecond laser pulse irradiations in air environment [7–11]. Their orientation is perpendicular to the laser beam polarization and the periods typically range between $\sim 0.6\lambda$ and λ , depending on the degree of material excitation [10,12], and the number of laser pulses per spot [11]. Several authors have suggested that these structures are caused by excitation of surface plasmon polaritons (SPP) at the air - silicon interface when the material turns from a semiconducting into a metallic state [2,10,13]. The interference between the electromagnetic field of the SPP and the incident laser pulse leads to a spatially modulated deposition of optical energy to the electronic system of the material. After coupling to the lattice system [14] and subsequent ablation processes, this results in a periodically corrugated surface topography [15].

The SPP-hypothesis has led to recent experiments investigating the impact of a temporally tailored energy distribution to the silicon surface by double-pulse irradiation [15–17]. In this material, the LSFL spatial period does not significantly depend on the double-pulse delay Δt [15,17],

while the LSFL rippled area strongly decreases with delays up to several ps [16]. Two characteristic exponential decay times of ~ 0.15 ps and ~ 11 ps were found.

In a numerical study, we have demonstrated that the SPP active area caused by a spatially Gaussian beam profile quantitatively explains the LSFL-covered (rippled) area as a function of the double-fs-pulse delay [18]. In this work, we extend the latter study and detail the contributions of the individual carrier generation and relaxation processes i.e., one- and two-photon absorption, carrier collisions and diffusion, and Auger recombination.

2 Theoretical model

For SPP excitation, the silicon has to turn from a semiconducting to a metallic state upon fs-laser excitation, the following criterion has to be fulfilled [19]

$$\Re[\varepsilon_{Si}^*] < -1. \quad (1)$$

Here, ε_{Si}^* represents the dielectric function of the laser-excited silicon which can be described (as a function of laser-induced carrier density N_e) by a Drude model [20]

$$\varepsilon_{Si}^*(N_e) = \varepsilon_{Si} - \frac{\omega_p^2(N_e)}{\omega^2(1 + i\frac{\nu}{\omega})}, \quad (2)$$

where $\omega_p = \sqrt{\frac{N_e e^2}{m_e^* \varepsilon_0}}$ represents the plasma frequency and ω the laser angular frequency [e : electron charge, ε_0 : dielectric permittivity of the vacuum].

The temporal change of the carrier density in the conduction band $\frac{\partial N_e}{\partial t}$ is described by a nonlinear partial differential equation (Eq. 3) considering carrier generation, carrier diffusion and Auger recombination. The carrier diffusion is driven by its temperature T_e , which couples via electron-phonon (e-ph) interaction with the silicon lattice temperature T_{Si} and is described by a two-temperature model (Eqs. 4, 5).

$$\frac{\partial N_e}{\partial t} = \underbrace{\nabla(k_B T_e \mu_e \nabla N_e)}_{\text{carrier diffusion}} + \underbrace{G_e}_{\text{generation}} - \underbrace{R_e}_{\text{recombination}} \quad (3)$$

$$C_{Si} \frac{\partial T_{Si}}{\partial t} = \nabla(\kappa_{Si} \nabla T_{Si}) + \gamma(T_e - T_{Si}) \quad (4)$$

$$C_e \frac{\partial T_e}{\partial t} = \underbrace{\nabla(\kappa_e \nabla T_e)}_{\text{heat diffusion}} - \underbrace{\gamma(T_e - T_{Si})}_{\text{e-ph coupling}} + \underbrace{Q_e}_{\text{heat source}} \quad (5)$$

The carrier generation rate is given by $G_e = \frac{\sigma_1 I}{\hbar \omega} + \frac{\sigma_2 I^2}{2\hbar \omega}$, the Auger recombination rate by $R_e = \frac{N_e}{\tau_{AR} + (C_{AR} N_e^2)^{-1}}$ and the heat source term is $Q_e = (\hbar \omega - E_g) \frac{\sigma_1 I}{\hbar \omega} + (2\hbar \omega - E_g) \frac{\sigma_2 I^2}{2\hbar \omega}$

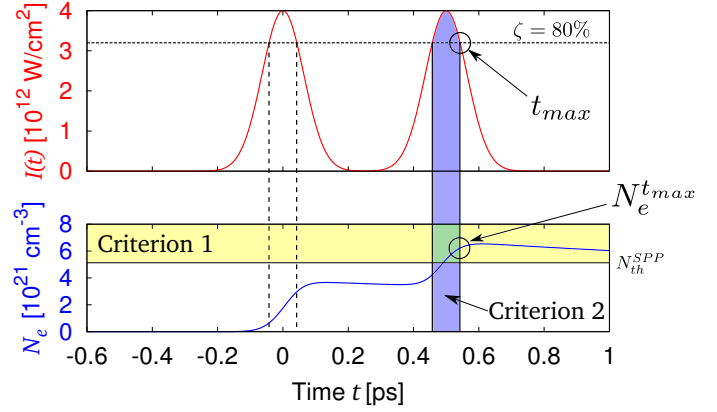


Fig. 1 Illustration of the two SPP excitation criteria (as discussed in the text). The upper part shows the intensity profile of a double-pulse (Eq. 6) with $\Delta t = 0.5$ ps, $\tau = 150$ fs and $F_0 = 0.3$ J/cm². The lower part represents a numerical calculation of the corresponding carrier density. The colored regions indicate the regimes where the criteria are satisfied individually. t_{max} defines the last moment when both criteria are fulfilled simultaneously.

$+ E_g R_e - \frac{3}{2} k_B T_e \frac{\partial N_e}{\partial t}$. The carrier mobility $\mu_e = e/(m_e^* \nu)$ depends on the collision frequency ν . The relevant parameters are compiled in Tab. 1.

The intensity $I(t, z)$ in the sample is calculated by numerically solving the equation $\frac{\partial I}{\partial z} = -(\sigma_1 I + \sigma_2 I^2)$. At the sample surface, it is calculated via $I(t, z=0) = [1 - R] I_0(t)$, where R is the transient surface reflectivity at $\lambda = 800$ nm [27]. For a temporally Gaussian double-pulse, the incident laser intensity I_0 is given by

$$I_0(t) = \frac{F_0}{\tau} \sqrt{\frac{4 \ln 2}{\pi}} \left[e^{-\frac{1}{2} \left(\frac{t}{\sigma\tau}\right)^2} + e^{-\frac{1}{2} \left(\frac{t-\Delta t}{\sigma\tau}\right)^2} \right], \quad (6)$$

where F_0 denotes the peak fluence of each individual pulse of the sequence. For more details on the model, refer to Refs. [18, 28].

Two criteria must be satisfied to allow the excitation of Surface Plasmon Polaritons (SPPs). *Criterion 1* is defined by the condition that carrier density must exceed a threshold density N_{th}^{SPP} defined by Eq. (1). Combining Eqs. (1) and (2), this threshold density can be rewritten as [13]

$$N_{th}^{SPP} = \frac{m_e^* \varepsilon_0 (\Re[\varepsilon_{Si}] + 1)}{e^2} (\omega^2 + \nu^2). \quad (7)$$

Criterion 2 is based on the idea that temporal interference between the incident laser wave and the SPP is required (which occurs lastly during the second part of the double-pulse). This defines the last instant t_{max} where the intensity of the second pulse drops to a fraction ζ of its maximum value [$I_0(t_{max}) = \zeta \times \max\{I_0(t)\} = \zeta \times F_0/\tau \times \sqrt{4 \ln 2/\pi}$]. Both criteria are illustrated in Fig. 1 where the intensity distribution of the double-pulse sequence is shown in the upper part, and the corresponding carrier dynamics is presented in the lower part. ζ is exemplified for a value of 80%, and the corresponding t_{max} is indicated by the two circles.

Coefficient	Symbol	Value	Unit	Reference
Band gap energy	E_g	1.12	eV	[21]
Dielectric constant of crystalline silicon	ϵ_{Si}	$13.64 + 0.048i$	—	[22]
One-photon absorption coefficient	σ_1	1.021×10^5	m^{-1}	[22]
Two-photon absorption coefficient	σ_2	6.8×10^{-11}	m^2/W	[23]
Carrier collision time	ν^{-1}	1.1×10^{-15}	s	[20]
Effective optical mass	m_e^*	1.64×10^{-31}	kg	[20]
Auger recombination rate	C_{AR}	3.8×10^{-43}	m^6/s	[24]
Minimum Auger recombination time	τ_{AR}	6.0×10^{-12}	s	[25]
Minimum electron-phonon coupling time	τ_{γ}^0	240×10^{-15}	s	[26]
Threshold density for electron-phonon coupling	N_{th}	6.02×10^{26}	m^{-3}	[26]

Table 1 Material parameters used in the numerical simulations of femtosecond laser-irradiated silicon (wavelength $\lambda = 800$ nm, pulse duration $\tau = 150$ fs).

In order to consider the spatially Gaussian beam profile used in the experiments [16], the corresponding radial distribution of the carrier density has to be calculated. For that, the Eqs. (3-5) have been simultaneously solved numerically for different fluences and delays. The radial position r of the Gaussian beam is linked to the local laser fluence F by the relation $F(r) = F_0 \exp[-2(r/w_0)^2]$. Thus, the radial position r can be associated with $N_e^{tmax}(t, \Delta t, F_0)$. Applying now the threshold criterion (Eq. 7) allows to quantify the SPP active area \mathcal{A}_{SPP} , as illustrated in Fig. 2. By systematically varying Δt for the given experimental conditions, a comparison between the SPP active area \mathcal{A}_{SPP} and the LSFL-rippled area \mathcal{A}_{LSFL} can be performed as discussed in the following section.

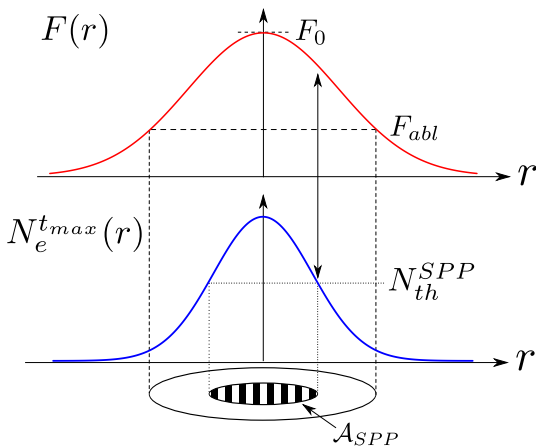


Fig. 2 Scheme of the evaluation of the SPP active area \mathcal{A}_{SPP} considering the spatially Gaussian beam profile (upper part), and the corresponding radial carrier density distribution (lower part). Each radial position of the Gaussian beam can be associated with a carrier density N_e^{tmax} which respects the temporal interference criterion. The threshold density for SPP excitation N_{th}^{SPP} then defines \mathcal{A}_{SPP} .

3 Results

In order to quantify the impact of the optical absorption, Auger recombination and carrier diffusion, all of these processes have been studied individually. For each case, starting from the optimum agreement demonstrated in Ref. [18], the corresponding process parameter (two-photon absorption: σ_2 , Auger recombination: R_e , carrier diffusion: μ_e) has been varied while keeping the others unchanged.

Fig. 3 shows the SPP active area \mathcal{A}_{SPP} as a function of the double-pulse delay Δt up to 3.5 ps for three different values of two-photon absorption coefficient $\sigma_2 = 0, 2.5$ and 6.8 cm/GW. The results of the numerical calculations are shown as lines, while the LSFL rippled area is added as blue data points for comparison. The black solid line represents the optimum agreement between \mathcal{A}_{SPP} and \mathcal{A}_{LSFL} . For $\sigma_2 = 0$ (i.e., one-photon absorption only), the results do not reproduce the rapid decay of LSFL-rippled area at short pulse delays. Moreover, to obtain an optimum agreement with \mathcal{A}_{LSFL} at longer delays, the peak fluence had to be set to $F_0 = 1.6$ J/cm², which is 10 times higher than the experimental value $F_0^{exp} = 0.15$ J/cm² [16]. In order to quantify the importance of the two-photon absorption, σ_2 has been varied between the two most prominent values found in the literature, i.e., $\sigma_2 = 2.5$ cm/GW [29] and $\sigma_2 = 6.8$ cm/GW [23]. However, no significant differences can be observed when the peak fluence is adjusted individually for an optimum agreement ($F_0 = 0.67$ J/cm² for $\sigma_2 = 2.5$ cm/GW and $F_0 = 0.40$ J/cm² for $\sigma_2 = 6.8$ cm/GW). The choice of the latter is more reasonable here as its corresponding fluence is closer to the experimental value. These results demonstrate that the two-photon absorption is essential to explain the rapid decay of \mathcal{A}_{SPP} .

In order to quantify the impact of Auger recombination, the Auger recombination rate has been set to $R_e = 0$. Fig. 4 shows the SPP active area \mathcal{A}_{SPP} as a function of the double-pulse delay Δt with (solid line) and without (dotted line) Auger recombination. For $R_e = 0$ and temporally non-

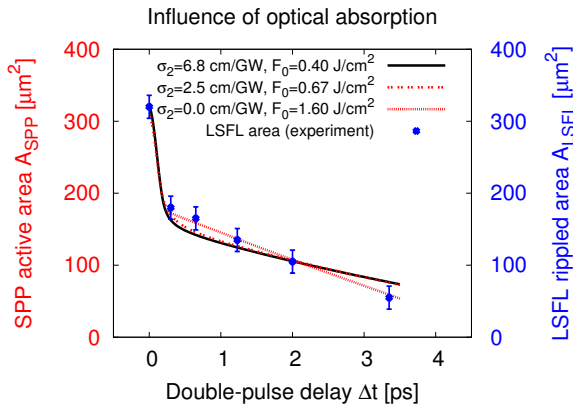


Fig. 3 SPP active area as a function of double-pulse delay for different values of two-photon absorption coefficient σ_2 . F_0 has been adjusted for an optimum agreement with experiments. In all cases, ζ has been fixed to 99%.

overlapping double-pulses, the SPP active area remains almost constant, indicating that diffusion cannot significantly reduce the laser-induced carrier density on a timescale of a few ps. The case with Auger recombination included ($R_e \propto N_e^3$) clearly demonstrates the major contribution of this effect to the SPP active area.

In order to study the effect of carrier diffusion, the carrier mobility μ_e was varied. Fig. 5 shows the SPP active area \mathcal{A}_{SPP} as a function of the double-pulse delay Δt for two different carrier mobilities μ_e . The best agreement (black curve) with \mathcal{A}_{LSFL} has been obtained by setting $\mu_e = e/(m_e^*v) = 10.7 \text{ cm}^2/(\text{Vs})$ [18], resulting from the carrier collision time $\nu^{-1} = 1.1 \text{ fs}$ reported in Ref. [20]. The dotted curve has been calculated by setting $\mu_e = 0$. This comparison demonstrates the limited influence of carrier diffusion on SPP active area on the timescale up to a few ps.

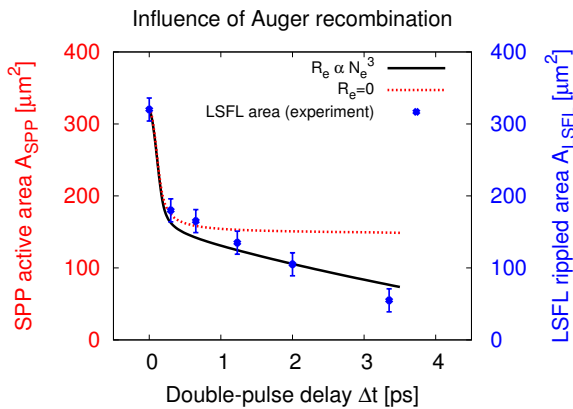


Fig. 4 SPP active area as a function of double-pulse delay for Auger recombination included and excluded ($R_e = 0$). In both cases, ζ has been fixed to 99% and $F_0 = 0.40 \text{ J/cm}^2$.

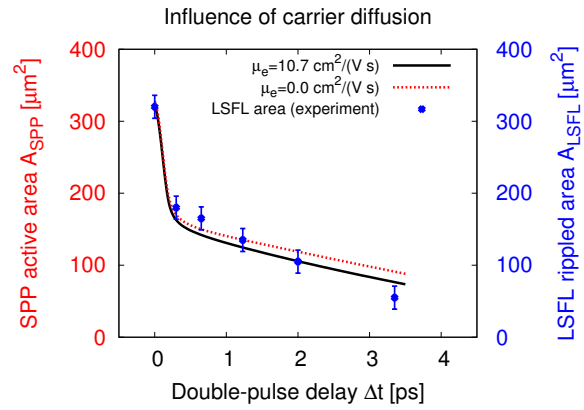


Fig. 5 SPP active area as a function of double-pulse delay for two different carrier mobilities μ_e . In all cases, ζ has been fixed to 99% and $F_0 = 0.40 \text{ J/cm}^2$.

4 Conclusion

The carrier dynamics at the surface of silicon upon femtosecond double-laser pulse irradiation has been numerically investigated as a function of double-pulse delay and laser peak fluence, considering different processes of carrier generation and relaxation. Based on that and on two optical criteria, the SPP active area was quantified. The comparison to experimental results of the LSFL rippled area confirms the SPP-based mechanism of LSFL formation. It was quantitatively demonstrated that the two-photon absorption is responsible for the fast decay in the sub-picosecond delay range of the SPP active area, while Auger recombination accounts for the slower area decay at delays up to several picoseconds. Diffusion plays a minor role only.

Acknowledgements T.J.-Y.D. acknowledges a postdoctoral fellowship awarded by the Adolf-Martens-Fond e.V. This work was supported by the German Science Foundation (DFG) under Grant Nos. RO 2074/7-2 and KR 3638/1-2.

References

1. A. Borowiec, H.K. Haugen, Appl. Phys. Lett. **82**(25), 4462 (2003)
2. M. Huang, F. Zhao, Y. Cheng, N. Xu, Z. Xu, ACS Nano **3**(12), 4062 (2009)
3. U. Chakravarty, R. Ganeev, P. Naik, J. Chakera, M. Babu, P. Gupta, J. Appl. Phys. **109**, 084347 (2011)
4. J. Bonse, J. Krüger, S. Höhm, A. Rosenfeld, J. Laser Appl. **24**(4), 042006 (2012)
5. J.E. Sipe, J.F. Young, J. Preston, H.V. Driel, Phys. Rev. B **27**(2), 1141 (1983)
6. A.M. Bonch-Bruевич, M.N. Libenson, V.S. Makin, V.A. Trubaev, Opt. Eng. **31**(4), 718 (1992)
7. J. Bonse, S. Baudach, J. Krüger, W. Kautek, M. Lenzner, Appl. Phys. A **74**, 19 (2002)
8. F. Costache, S. Kouteva-Arguirova, J. Reif, Appl. Phys. A **79**, 1429 (2004)
9. M. Guillermin, F. Garrelie, N. Sanner, E. Audouard, H. Soder, Appl. Surf. Sci. **253**, 8075 (2007)

10. J. Bonse, A. Rosenfeld, J. Krüger, *J. Appl. Phys.* **106**, 104910 (2009)
11. J. Bonse, J. Krüger, *J. Appl. Phys.* **108**, 034903 (2010)
12. T.J.Y. Derrien, T.E. Itina, R. Torres, T. Sarnet, M. Sentis, *J. Appl. Phys.* **114**, 083104 (2013)
13. G.A. Martsinovskii, G.D. Shandybina, D.S. Smirnov, S.V. Zabolotnov, L.A. Golovan, V.Y. Timoshenko, P.K. Kashkarov, *Opt. Spectrosc.* **105**, 67 (2008)
14. T.J.Y. Derrien, T. Sarnet, M. Sentis, T.E. Itina, *J. Optoelectron. Adv. Mater.* **12**(3), 610 (2010)
15. M. Barberoglou, G. Tsiibidis, D. Gray, E. Magoulakis, C. Fotakis, E. Stratakis, P. Loukakos, *Appl. Phys. A* **113**, 273 (2013)
16. S. Höhm, A. Rosenfeld, J. Krüger, J. Bonse, *Appl. Surf. Sci.* **278**, 7 (2013)
17. S. Höhm, M. Rohloff, A. Rosenfeld, J. Krüger, J. Bonse, *Appl. Phys. A* **110**, 553 (2013)
18. T.J.Y. Derrien, J. Krüger, T.E. Itina, S. Höhm, A. Rosenfeld, J. Bonse, *Opt. Express* (Accepted) (2013)
19. H. Raether, *Surface Plasmons on Smooth and Rough Surfaces and on Gratings* (Springer-Verlag, 1986)
20. K. Sokolowski-Tinten, D. von der Linde, *Phys. Rev. B* **61**, 2643 (2000)
21. D. Bäuerle, *Laser Processing and Chemistry*, 4th edn. (Springer-Verlag, 2011)
22. E.D. Palik, *Handbook of Optical Constants of Solids* (Academic Press, 1985)
23. A. Sabbah, D. Riffe, *Phys. Rev. B* **66**, 165217 (2002)
24. H.V. Driel, *Phys. Rev. B* **35**(15), 8166 (1987)
25. E.J. Yoffa, *Phys. Rev. B* **21**(6), 2415 (1980)
26. T. Sjödin, H. Petek, H.L. Dai, *Phys. Rev. Lett.* **81**(25), 5664 (1998)
27. N.M. Bulgakova, R. Stoian, A. Rosenfeld, *Quantum Electron.* **40**(11), 966 (2010)
28. N.M. Bulgakova, R. Stoian, A. Rosenfeld, I.V. Hertel, W. Marine, E.E.B. Campbell, *Appl. Phys. A* **81**, 345 (2005)
29. A.D. Bristow, N. Rotenberg, H.M.V. Driel, *Appl. Phys. Lett.* **90**, 191104 (2007)